Research Square

Preprints are preliminary reports that have not undergone peer review.
They should not be considered conclusive, used to inform clinical practice,
or referenced by the media as validated information.

Reference frames reverse biases in human heading perception

Renate Reisenegger

tate.reisene@gmail.com

Applied Physics and Neurophysics, University of Marburg https://orcid.org/0009-0008-4465-4520

Michael Hahn

Saarland University https://orcid.org/0000-0003-4828-4834

Ambika Bansal

Center for Vision Research, York University

Narges Salehi

Applied Physics and Neurophysics, University of Marburg

Laurence Harris

York University https://orcid.org/0000-0002-7154-8757

Frank Bremmer

Philipps-Universität Marburg https://orcid.org/0000-0003-1597-7407

Article

Keywords: Heading perception, optic flow, self-motion, reference frames, EEG, Bayesian causal inference

Posted Date: October 5th, 2026

DOI: https://doi.org/10.21203/rs.3.rs-10966727/v1

License: This work is licensed under a Creative Commons Attribution 4.0 International License.
Read Full License

Additional Declarations: There is **NO** Competing Interest.

Reference frames reverse biases in human heading perception

Renate Reisenegger[1,2,*], Michael Hahn[3], Ambika Bansal[4], Narges Salehi[1,2], Laurence R. Harris[4], & Frank Bremmer[1,2,6]

[1] Applied Physics and Neurophysics, University of Marburg, Karl-v-Frisch Str 8a, 35043 Marburg, Germany

[2] Center for Mind, Brain and Behavior, Universities of Marburg, Giessen, and Darmstadt, Hans-Meerwein-Str. 6, 35032 Marburg, Germany

[3] Saarland University, Saarbrücken, Germany

[4] Center for Vision Research, York University, Toronto, Ontario, Canada

[6] Department of Physiology, School of Biomedical Sciences, Monash University, Clayton, Victoria, Australia

Correspondence to:

renate.reisenegger@physik.uni-marburg.de

Abstract

As observers move through the world, optic flow provides critical information about self-motion, including direction (heading). Over the years, studies of heading perception have reported conflicting biases: some toward straight ahead (centripetal), others away from it (centrifugal). We hypothesize that these discrepancies arise from differences in the reference frame used to report heading. We tested this hypothesis using a unique “Edgeless Graphics Geometry” (EGG) display with an ultra-wide (~224°) field of view. Participants viewed brief optic flow stimuli simulating self-motion across a ground plane. They reported heading either egocentrically (relative to themselves) or allocentrically (relative to external space). In the same observers and despite identical response ranges (±110°), egocentric reports exhibited a robust bias towards straight ahead, whereas allocentric reports showed a pronounced bias away from straight ahead. These differences suggest a reference-frame–dependent coordinate transformation of visual self-motion signals dependent on the task in hand. To identify neural correlates of this transformation, we combined a two alternative forced choice heading task with non-invasive scalp EEG. Following stimulation, participants were cued to respond in either an egocentric or an allocentric reference frame. Allocentric responses were associated with a stronger post-cue increase in theta-band power than egocentric responses, suggesting differential retrosplenial and (para-)hippocampal networks’ involvement in these two types of response preparation. Finally, a Bayesian causal inference model captured both these behavioral and neural findings, providing a principled account of how reference-frame transformations generate opposing biases in heading perception, thereby resolving a long-standing issue in vision science.

Keywords

Heading perception, optic flow, self-motion, reference frames, EEG, Bayesian causal inference.

Introduction

As we navigate through the world, our visual system continuously processes optic flow[1,2], the visual stimulus generated by our own displacement through the environment. Optic flow provides essential information about self-motion, allowing the estimation of the direction of movement (heading)[3,4], relative speed[5–7], and travel distance[8–10] (for a review see: e.g.[11]). Among these, heading perception, the ability to determine one's direction of motion, has been a central topic in the study of self-motion processing. Understanding how the brain extracts heading information from optic flow is critical not only for basic vision science but also for understanding navigation and visuomotor control.

Early research established that humans can reliably judge heading direction from optic flow even when the retinal flow is further complicated by eye or head movements[3,12]. However, several studies have revealed systematic biases in heading estimates, which often appear contradictory. Specifically, some experiments report a centripetal bias, where perceived heading is shifted toward the straight-ahead direction[13–20], while others observe the opposite, a centrifugal bias, in which heading is perceived as farther away from straight ahead than it actually is[21–23]. Given the central role of understanding self-motion perception in vision science, this gap in understanding is remarkable.

Sun and colleagues [24] recently suggested that the seemingly contradictory results (centripetal vs. centrifugal heading bias) arise from the response range given to participants in the respective studies. The authors proposed that when participants make heading judgments over a narrow range of possible directions, centripetal biases emerge, whereas larger response ranges induce centrifugal biases. This explanation emphasizes the geometry of the response mapping rather than underlying perceptual, neural or computational factors. However, we believe that systematic differences between experiments extend beyond or even override possible effects resulting from response ranges[25]. Studies reporting centripetal biases typically require participants to indicate perceived heading on a horizontal line representing an egocentric (participant-centered) perspective. On the contrary, studies reporting centrifugal biases often provide a "bird's-eye" view for response, where participants indicate their heading as an angle on a circle or arc in an allocentric (world-centered) perspective.

This observation suggests an alternative explanation: the reference frame in which the response is performed, egocentric vs. allocentric, may be a key determinant of heading perception biases.

Reference frame transformations are fundamental to spatial cognition, enabling the translation of sensory information between self-centered and world-centered coordinates (for a review see: e.g. [26]). In the context of self-motion perception, adopting an allocentric reference frame requires additional neural computations beyond those required for egocentric judgments[27–30], potentially introducing systematic perceptual shifts. To directly test this hypothesis at the perceptual level, we used the Edgeless Graphics Geometry (EGG) display, which provides an exceptionally wide field of view (~224° on the horizontal plane) without visible borders. This setup allows a wide response range for the egocentric condition (and essentially the same as in the allocentric condition), usually not possible with common displays, while minimizing edge-based reference cues. Participants viewed brief (600 ms) optic flow stimuli simulating self-motion across a ground plane from an egocentric perspective and indicated their perceived heading in three conditions: (i) Egocentric: report on a horizontal line corresponding to the frontal visual field, (ii) Allocentric arc: report as an angle on a "bird's-eye view" arc display, and (iii) Allocentric circle: report as an angle on a "bird's-eye view" full circular display.

The first two conditions shared the same large response range (±110°), eliminating response-range differences as a confounding factor, while the third one comprised the maximum possible ±180° range. We predicted that if response range were the main driver of heading bias, all conditions should yield centrifugal biases, with the first two conditions (with the identical response range) inducing a very similar bias, and the bias being increased for the third (allocentric circle) condition. Conversely, if the reference frame plays a central role, we would expect opposite bias directions between egocentric and allocentric conditions (centripetal and centrifugal, respectively).

To investigate the neural correlates of these biases, we conducted a second experiment employing a perceptual paradigm on a standard computer display and concurrent electroencephalography (EEG) recordings. Participants performed a two-alternative forced-choice (2AFC) task, deciding whether a previously seen heading was to the left or right of a probe. The response had to be given either in an egocentric (horizontal line) or allocentric (arc) format and was instructed by a cue. Based on prior work implicating the retrosplenial cortex (RSC) and (para-) hippocampal regions in reference frames transformations from egocentric to allocentric[26,31–34], we hypothesized that allocentric judgments would elicit stronger oscillatory activity between 2 and 14 Hz, usually referred to as theta band in hippocampal research (also referred to as delta (1-4 Hz), theta (4-8 Hz) and alpha (8-12 Hz) in human EEG research), reflecting the engagement of spatial transformation networks.

Finally, we modeled our behavioral data based on the unifying theory presented in Hahn & Wei[35]. By fitting the egocentric and allocentric arc conditions, we aimed to reconstruct the specific resources allocations (of neural populations) and prior distributions required to produce the observed behavioral biases. Our goal was to look beyond the surface-level responses to characterize how the brain processes identical visual stimuli across different tasks. By extracting these latent components, we aimed to understand and explain how the internal representation of self-motion is altered to meet the specific demands of each reference frame.

Results

Experiment 1A

Participants were shown self-motion stimuli with a heading ranging from -55° to 55° and were asked to report in which direction they were virtually moving. Negative values indicate forward-leftward heading, positive values forward-rightward headings and 0° corresponds to straight-ahead. In a given trial, one of three response options was provided: a horizontal line across the screen where participants had to report their perceived heading from their own perspective (egocentric condition), or a circle or an arc where participants had to imagine a “bird’s eye” view perspective (allocentric circle and allocentric arc conditions, respectively) (Figure 1).

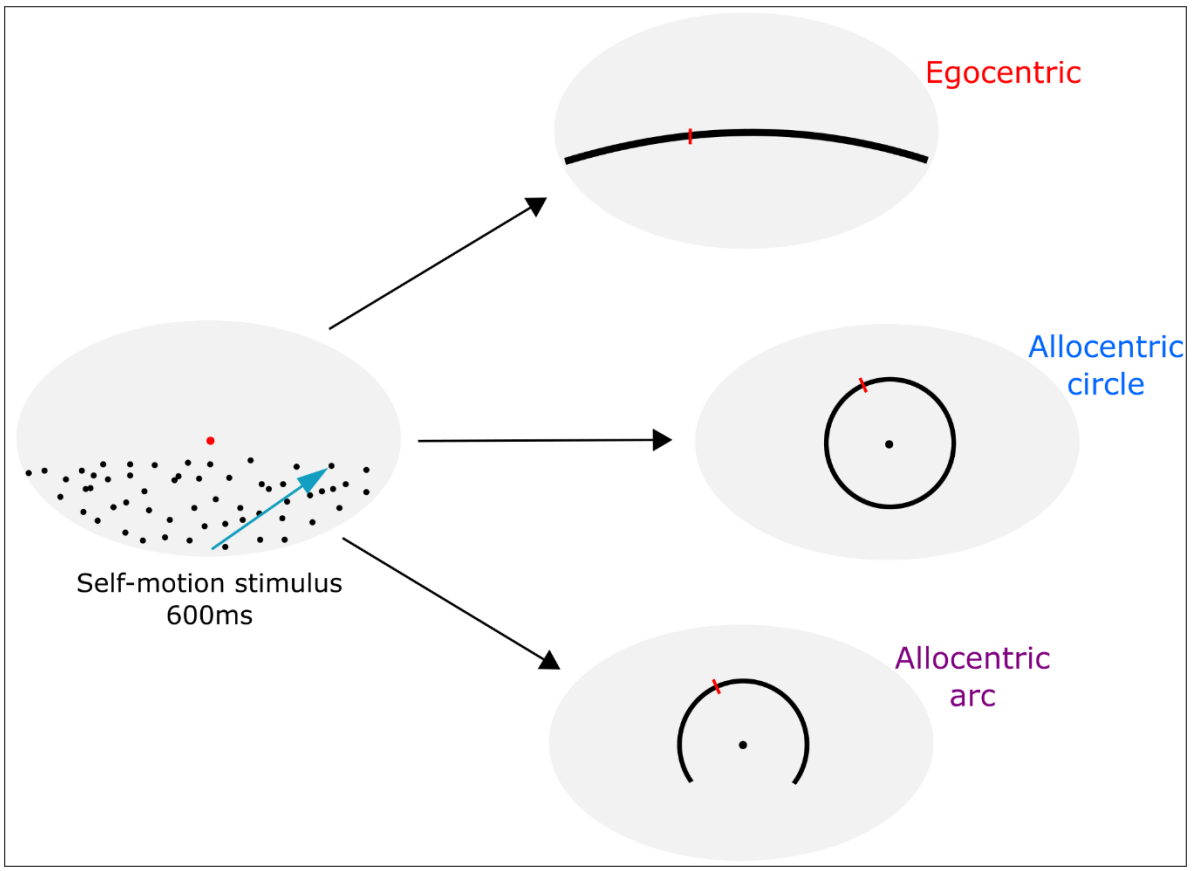


Figure 1. Behavioral experiment's paradigm.

Participants were shown a self-motion stimulus in a certain heading direction (between -55° and 55° for experiment 1A, and between -90° and 20° or between -20° and 90° in experiment 1B) for 600ms (blue arrow indicates a possible heading direction, it is not shown in the actual stimulus). Participants had to report the perceived heading in one of three different conditions: a) The egocentric condition consisted of a horizontal line in the form of an arc surrounding the participant, with the same distance to the participant at all points, that spread between -110° and 110° (the whole FOV). Participants had to adjust the red bar on the arc with the left stick of a wireless Xbox controller (Microsoft Xbox) and press Ⓐ when they thought they were pointing towards the previously seen heading. b) The allocentric circle condition consisted of a circle in front of the participant with a central dot. Participants were told they were seeing themselves from above ('Birds-eye-view') and had to point towards the angle they were heading in the previously seen self-motion. c) The allocentric arc condition consisted in the same arc as in the egocentric condition (±110°), but the arc was positioned in front of the participant and the instructions were the same as in the allocentric circle condition, with the addition of the arc corresponding to the arc they were shown in the egocentric condition. In both allocentric conditions, participants also had to use the left stick and Ⓐ to adjust the position of the bar and confirm its position.

In the first set of data collection, only the egocentric and allocentric circle conditions were used. In the second set the allocentric arc was introduced, explaining to the participants that the boundaries of the arc corresponded to the edges of the screen (which were beyond their field of view when looking straight-ahead).

Group data for both sets of data collection are shown in Figure 2 (also see Sup. Figure 1). Biases differed considerably between the egocentric and allocentric condition (Wilcoxon sign-rank test, corrected $p \leq 0.003$ for all headings, exact bias and p values in Table 1). For the egocentric condition we found no significant bias for the smallest eccentricity tested (10° eccentricity, $p = 1$) and a significant centripetal bias (bias towards the center) for all heading eccentricities beyond 10° (exact bias and p values in Table 2). In both allocentric conditions we found a significant centrifugal bias (Figure 2). The strength was modulated by eccentricity with a maximum around 20° - 40° (exact bias and p values for all headings in Table 2).

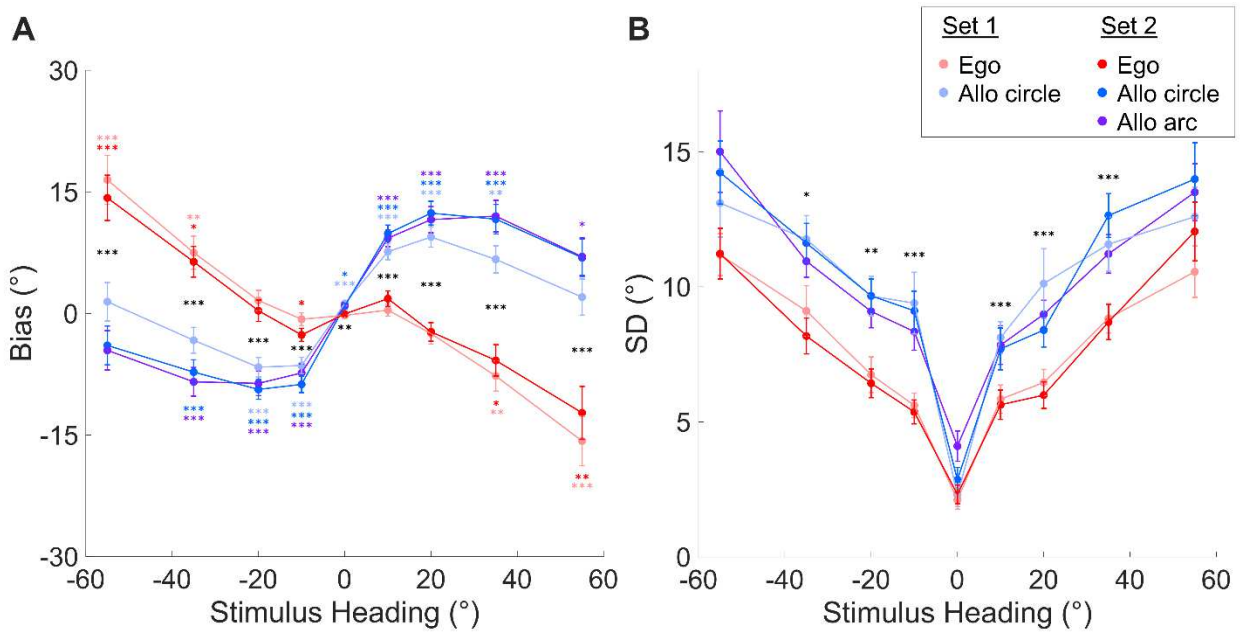


Figure 2. Bias and standard deviation of perceived heading (Experiment 1A, N = 37).

A*. Average bias across participants as a function of the stimulus heading (0° corresponds to straight-ahead, negative and positive headings correspond to headings towards the forward left and right, respectively).* ***B****. Standard deviation of the bias across participants as a function of the stimulus heading. In* ***A*** *and* ***B****, dots indicate mean values, error bars indicate standard error of the mean, across participants. Data from the egocentric condition are plotted using red-scale colors, and the allocentric arc condition using blue-scale colors. Within each color scale, stimulus ranges are depicted in bright to dark, corresponding to data from*

*Set 1 and Set 2, respectively. Colored asterisks indicate significant differences from zero (i.e. no bias) and black asterisks indicate significant differences between egocentric and allocentric circle conditions (Wilcoxon signed rank test with Bonferroni correction, ***: p<0.001. **: p<0.01. *: p<0.05). Wilcoxon signed rank test with Bonferroni correction showed no significant differences between Set 1 and 2 of the experiment (p>0.09).*

These results support the hypothesis of heading biases depending on reference frame transformations, given that the same response range caused significantly different biases by changing from an egocentric to an allocentric reference frame. On the other hand, both allocentric conditions (arc vs. circle) produced very similar biases despite different response ranges (220° vs 360°).

Experiment 1B

In the allocentric conditions of Experiment 1A, the centrifugal bias of perceived self-motion directions was decreasing towards the limits of presented headings (±55°). We aimed to understand if for even more eccentric headings this bias would eventually flip and become centripetal. To make results comparable regarding task load of participants, in Experiment 1B we presented the same range of headings (110°), but now centered on either side, left or right. Accordingly, as in Experiment 1A, participants were shown self-motion stimuli with a particular heading ranging this time, from either -90° to 20° (left-centered) or from -20° to 90° (right-centered). Each participant was presented with only one of the two ranges, either left-centered or right-centered. Like before, we asked participants to report their heading either from their own perspective (egocentric condition), or a “bird’s eye” view perspective (allocentric arc condition).

Results are shown in Figure 3. Like before, biases differed considerably between the egocentric and allocentric condition, being almost exclusively centripetal in the egocentric condition (exception only for the smallest eccentricity) (exact bias and *p* values in Table 3). Remarkably, for very eccentric headings, the bias in the allocentric condition became centripetal.

We believe this shift from centrifugal towards centripetal heading perception might be caused by a) boundary effects of the reporting range, which was closer to the stimulus range in this experiment (reporting range = ±110°; stimulus range up to ±90°, as compared to a stimulus range = ±55° in experiment 1A), and b) a shift in the experimental prior towards the left or the right. This hypothesis will be explored in detail below, with the results of our computational modeling.

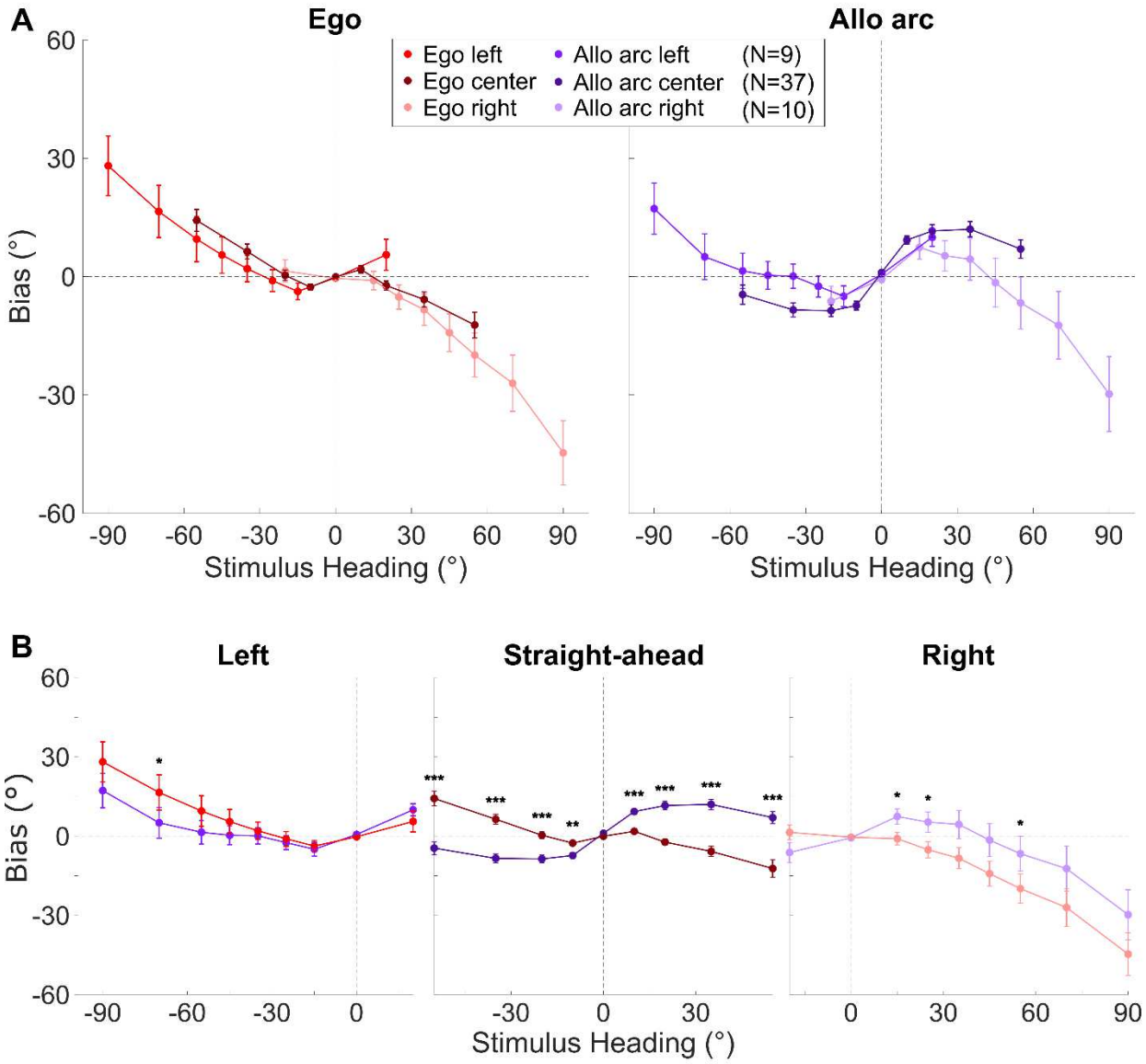


Figure 3. Bias in reported heading (Experiment 1B).

Mean reported bias across participants is shown as a function of the stimulus heading (0° = straight-ahead; negative and positive values indicate forward leftward and rightward headings, respectively). ***A*** *and* ***B*** *present the same dataset, grouped in two different ways: by reference frame condition (****A****) and by stimulus range (****B****). Data from the central stimulus range is taken from Experiment 1A. Each dot represents the mean across participants, and error bars denote the standard error of the mean. The egocentric condition is plotted using red-scale colors, and the allocentric arc condition using purple-scale colors. Within each color scale, stimulus ranges are depicted from bright to dark, corresponding to rightward, leftward, and centered*

*ranges, respectively. Asterisks indicate significant differences between egocentric and allocentric arc conditions (Wilcoxon signed rank test with Bonferroni correction, ***: p<0.001. **: p<0.01. *: p<0.05).*

EEG Experiment

Behavioral results

In the second part of our study, we aimed to discover a neural correlate of the observed heading biases. In a given trial, participants were first shown a self-motion stimulus with a certain heading (see Figure 4 for the experimental paradigm). Then, a probe was briefly flashed, and participants had to answer if the probe was displayed to the left or to the right of the previously seen heading. The probe was displayed in an egocentric or allocentric frame of reference and was instructed by a cue, presented directly after the self-motion stimulus for a variable duration (randomly chosen between 2200ms and 2800ms).

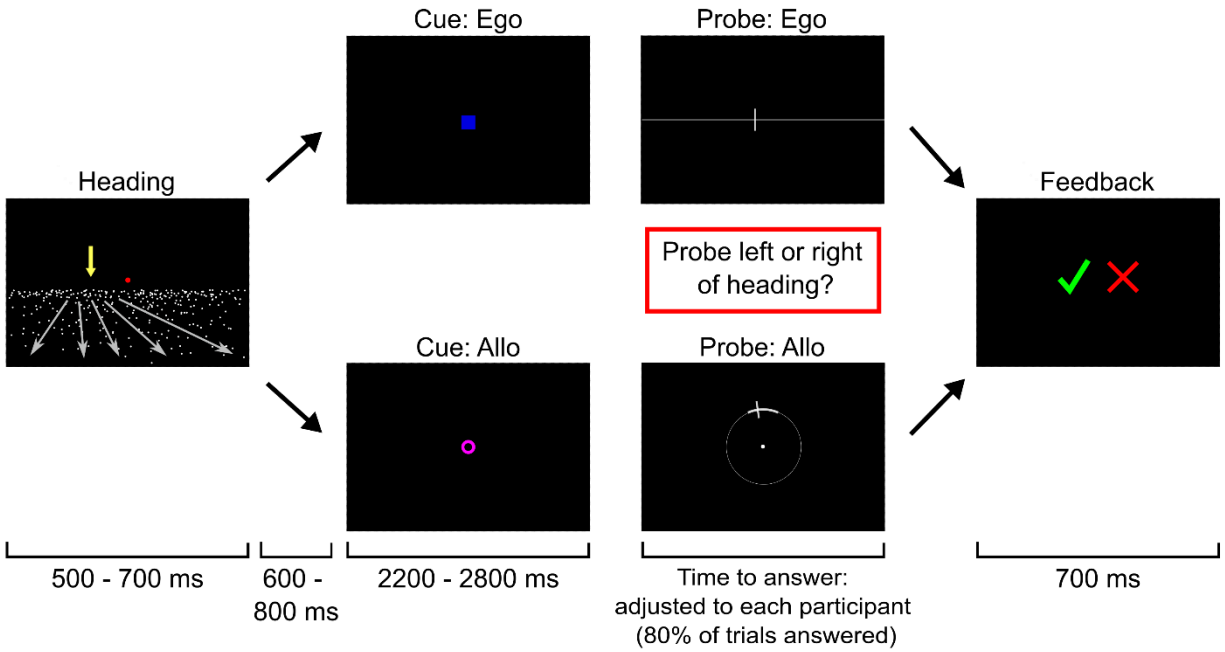


Figure 4. EEG experiment's stimulus trial.

Each trial consisted first of a stimulus (optic flow) simulating self-motion in a certain direction (heading) across a ground plane for 500 to 700 ms. It was followed by a cue period: a blue square for the egocentric condition (top row) and a magenta circle for the allocentric condition (bottom row), that lasted between 2200 and 2800 ms. A very short probe period followed thereafter, during which participants were instructed to

answer if the probe was displayed to the left or the right of the previously seen heading. The probe was shown either as a vertical bar on a horizontal line for the egocentric condition (top row) or as a bar on a circle with a bolded arc representing the size/width of the screen in that reference frame for the allocentric condition (bottom row). The duration was determined in a staircase approach for each participant until participants were able to answer about 80% of the trials before timing out. On average, the maximum duration of the presentation of the probe stimulus was around 460 ms. The trial ended with a feedback period of 700 ms where a green tick represented a correct trial and a red cross an incorrect one.

We first analyzed the proportion of trials that were answered either correctly, or incorrectly, or where the participants did not respond within a given time (timed-out). Proportion correct was significantly higher in the egocentric as compared to the allocentric condition (μ_{Ego} = 75.57±10.51%, μ_{Allo} = 67.22±8.67%, paired Wilcoxon rank test: p=0.0001). The opposite was found for the proportion of trials where participants did not respond in time (μ_{Ego} = 12.42±3.16%, μ_{Allo} = 20.46±2.1%, paired Wilcoxon rank test: p<0.0001). There was no significant difference in the fraction of incorrect trials between conditions (μ_{Ego} = 12.02±9%, μ_{Allo} = 12.32±8.32%, paired Wilcoxon rank test: p=0.9) (see Figure 5). This suggests that, behaviorally, the allocentric condition was more challenging than the egocentric condition, with the biggest difference being the time needed to give an answer.

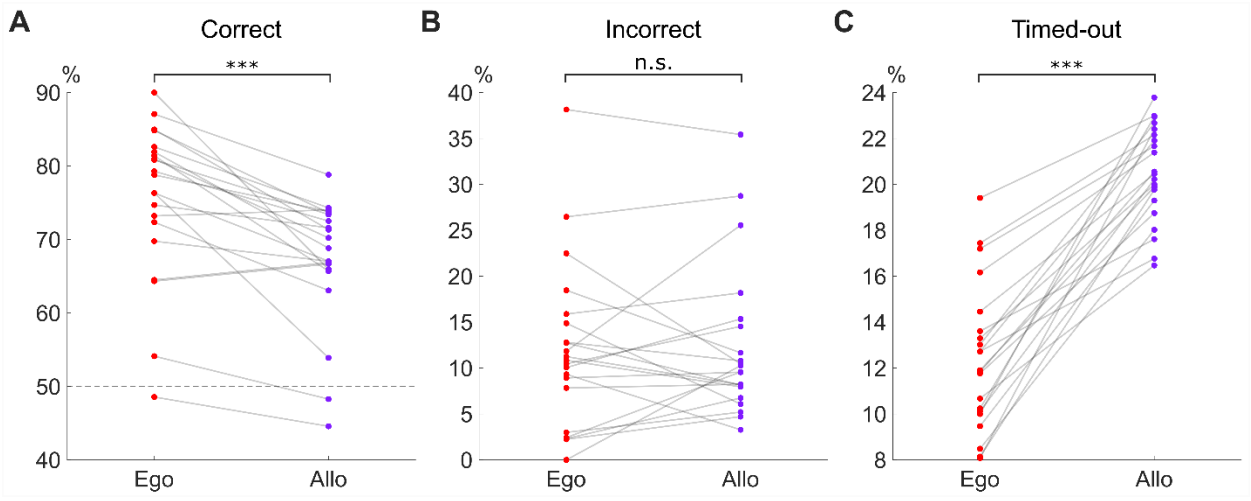


Figure 5. Behavioral performance of the EEG experiment.

Percentage of correct (A), incorrect (B) and timed-out (C) trials for each condition. (Trials where probe and stimulus heading were identical were excluded.) A pair of dots connected with a line represents the average result for a given participant tested in both conditions. A paired Wilcoxon signed rank test revealed significant differences between conditions in the correct and timed-out trials, but not in the incorrect trials

*(n.s.: p> 0.05. ***: p<0.001). Two participants showed a performance of less than 50% of the trials being correct. These two participants were excluded from the EEG analysis.*

In this part of our study, we provided feedback to the participants, which might have influenced the gain of their mapping from the stimulus to the different probes (ego- vs. allocentric). Therefore, we did not analyze possible behavioral reporting biases in this experiment.

Time-frequency results

For our EEG analysis we focused on the cue period, in which participants were instructed to give their upcoming response either in an ego- or allocentric reference frame.

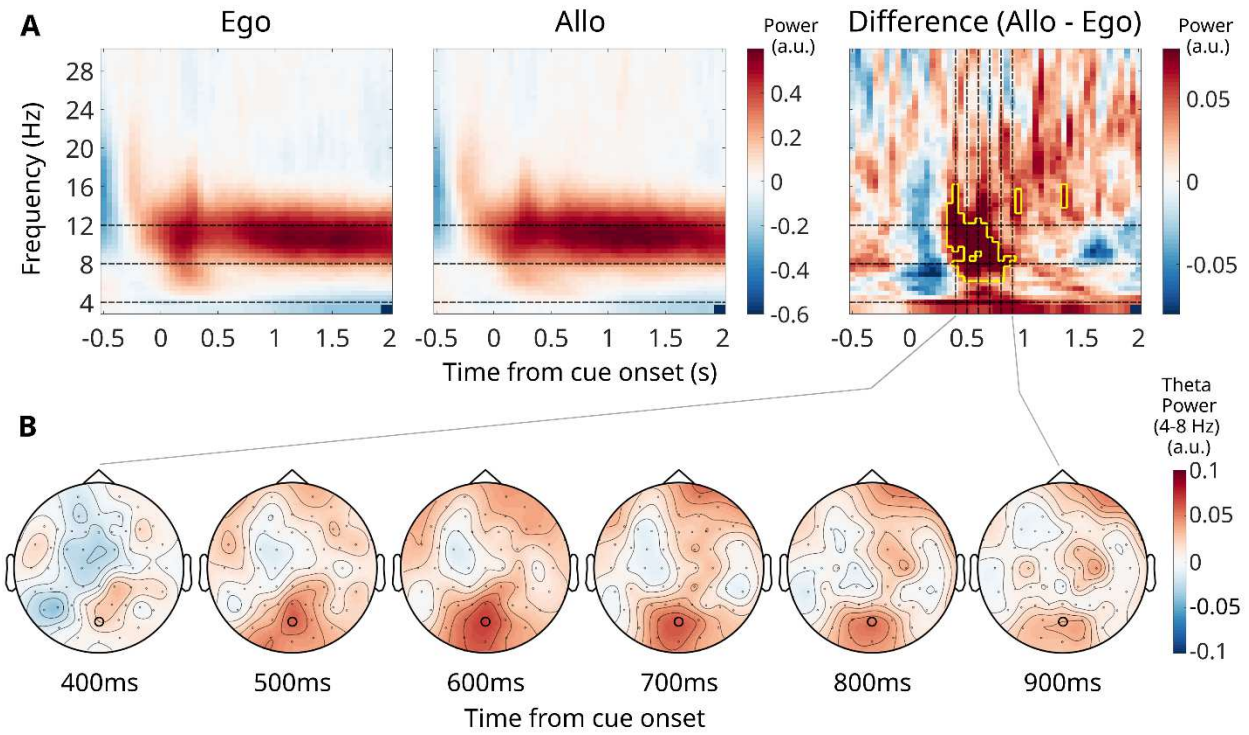


Figure 6. Time-frequency analysis of the ongoing EEG activity during the cue period (theta band).

A. *Time-frequency power spectra at electrode POz for the egocentric (left panel) and allocentric (center panel) conditions, along with their difference (allocentric - egocentric, right panel). Horizontal black lines indicate the boundaries of the theta (4-8 Hz) and alpha (8-12 Hz) frequency bands. Vertical black lines mark the time points shown in panel* ***B****. The yellow contours delineate the significant cluster identified by the cluster-based permutation test.* ***B.*** *Scalp topographies of theta-band activity from 400 to 900 ms after cue*

onset, displayed in 100 ms increments. Electrode POz is highlighted with a black circle. All time-frequency representations were first log-transformed (base 10) and subsequently z-scored relative to a pre-cue baseline period (-500 to -100 ms).

We found an increase in theta (4-8 Hz) and alpha (8-12 Hz) band power for both conditions (Figures 6 and 7) shortly after cue onset. We compared this power increase in both conditions with a cluster-based permutation analysis, which revealed a significant cluster from around 7 to 16 Hz at 450 to 900 ms after cue onset, indicating a significant increase in frequency power for the allocentric compared to the egocentric condition. Topo plots in Figures 6 and 7 show the increase in the respective power bands to be present mostly in the centro-parietal electrodes (POz, Pz and adjacent electrodes).

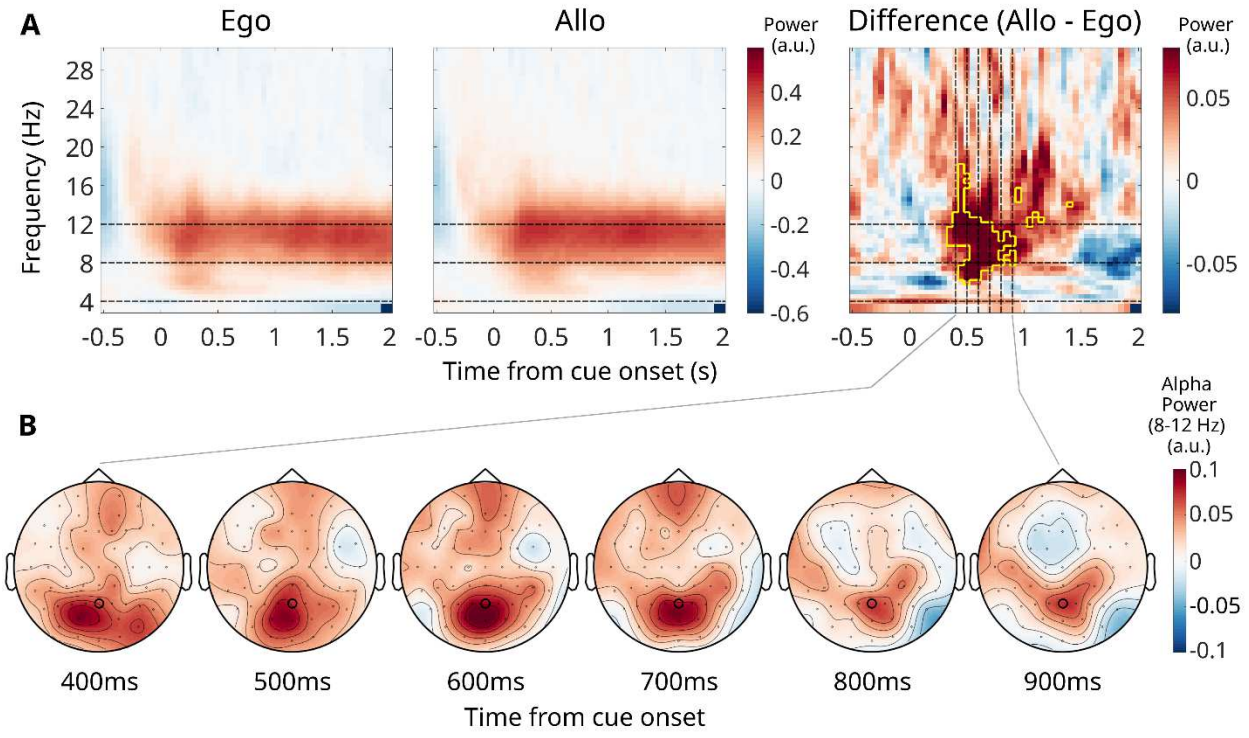


Figure 7. Time-frequency analysis of the ongoing EEG activity during the cue period (alpha band).

A. *Same depiction as in Figure 6, but now for data from electrode Pz.* ***B****. Same depiction as in Figure 6, but now for the alpha band (8-12 Hz) and electrode Pz.*

Modeling

As a final step to elucidate the mechanisms and potentially also the neural processing steps underlying the observed behavioral biases we used a computational model based on Bayesian causal inference, extending from the unifying theory of perceptual biased proposed by Hahn & Wei[35]. More specifically, this model attempts to reconstruct two latent components: a prior distribution, which generates an attractive bias towards its peak, and a so-called “resources” distribution, which generates a repulsive bias away from its peak. In our study, the experimental prior was given by the range and distribution of heading directions in the different experiments. The resources represent the square root of the population Fisher information and, as a coarse approximation, can thus be thought of as the derivative of tuning curves of populations of neurons responsive to visual self-motion stimuli[16,36,37]. This distribution determines the local precision of the sensory measurements across the stimulus space with high resources density indicating high sensitivity (low discrimination thresholds), while low density indicates low sensitivity (high thresholds). Together, these two biases are combined to generate the best fit to the behavioral biases found experimentally (more information in the Methods section).

To fit the model parameters, we used our behavioral data from Experiments 1A and 1B for the egocentric and the allocentric arc conditions. We evaluated several model configurations to identify the one that best captured the observed bias differences while maintaining biological plausibility. This process involved testing four primary constraints: (a) resources invariance across ranges, (b) resources invariance across conditions, (c) prior invariance across ranges (rotated by ±35°) and (d) prior invariance across conditions (see Modeling methods).

Constraint (c), the rotation of the prior to match the experimental shift while maintaining the shape of the prior constant, proved essential for the model to generate biologically plausible prior distributions. Consequently, it was maintained as a baseline for all subsequent configurations. Using only constraint (c) yielded a Negative Log-Likelihood (NLL) of 153.58. When adding resources invariance across ranges (constraint a), we observed a slight detriment to the model fit (NLL=155.04). However, the inclusion of resources invariance across conditions (constraint b), alongside constraints (a) and (c), resulted in the best performing model (NLL = 151.96), presumably by reducing overfitting through a more parsimonious parameter set. In contrast, requiring the prior to remain invariant across conditions (constraint d) led to a massive detriment in model fit (NLL = 186.52). Finally, combining the rotated prior (c) with resources invariance

across conditions (b) without enforcing resources invariance across ranges (a), resulted in a higher NLL (157.43) compared to models using constraints (c) alone or (c) and (a).

The model selection determined that the model that could best capture the differences in the biases between conditions while providing biologically plausible distributions, was achieved by constraining the prior for each condition to remain identical across stimulus ranges, except for a ±35° rotation corresponding to the experimental shifts and restraining the resources distributions to be the same across conditions and stimulus ranges (Figure 8). These results quantitatively demonstrate that while sensory resources can be treated as stable across conditions, condition-specific prior distributions are necessary to account for the observed behavioral data.

Note that because the EEG experiment (Experiment 2) utilized a 2AFC task rather than direct heading estimation, it was excluded from this modeling analysis.

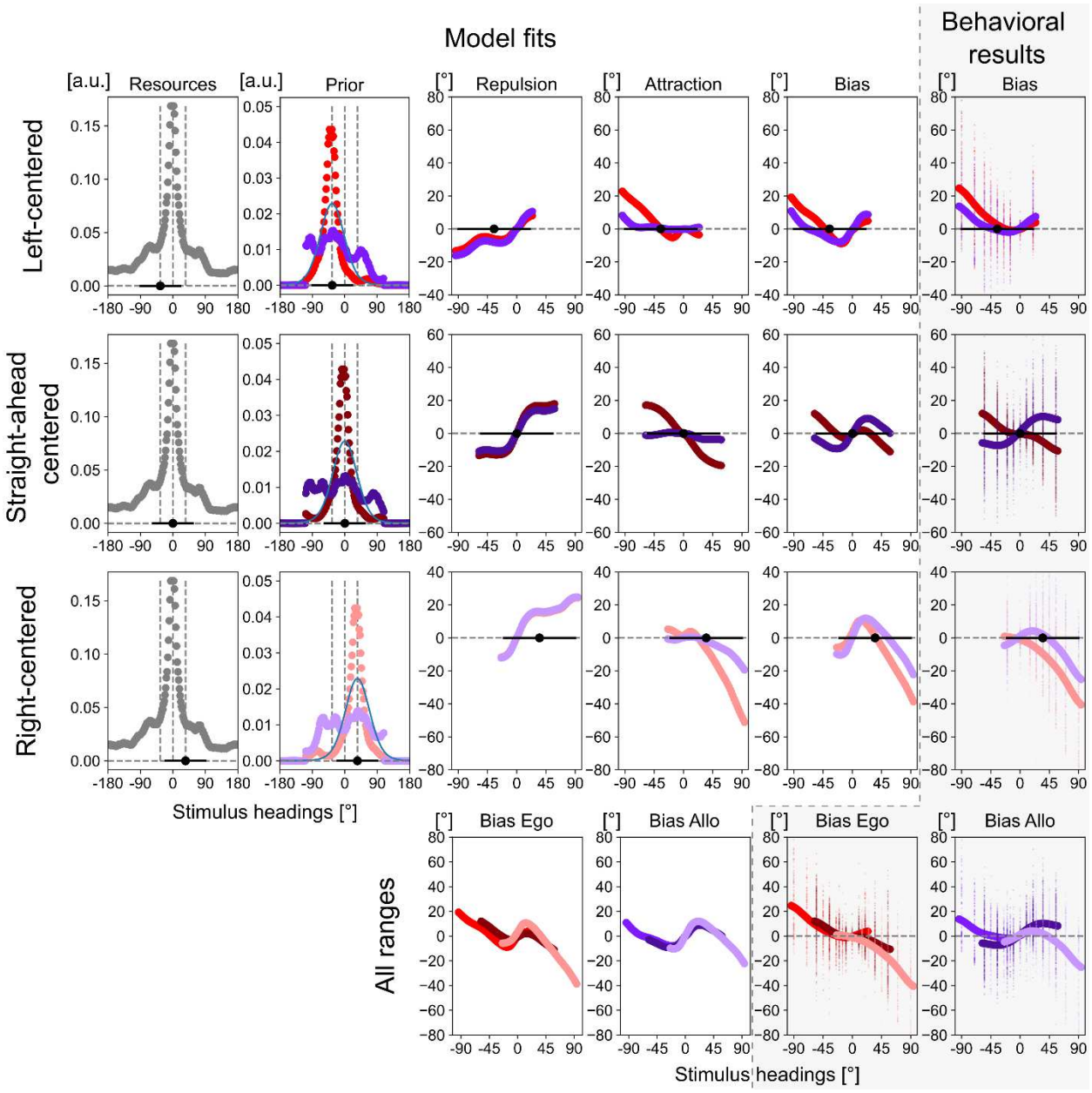


Figure 8. Best computational model fits.

Illustration of the modeling results constraining the resources to remain invariant across conditions and stimulus ranges, and the prior to remain constant but rotated by ±35°, organized by stimulus range across four rows. The first three rows depict the fits for the left-centered (-90° to 20°), straight-ahead centered (-55° to 55°), and right centered (-20° to 90°) ranges, respectively, while the bottom row provides a view of all three ranges superimposed for direct comparison. For the first three rows, from left to right, the columns show the model components, starting with the reconstructed resources (square root of the Fisher information) and prior distributions, followed by the repulsion and attraction biases they respectively generate, and the total bias ("weighted" combination of the repulsion and attraction biases). The final

column displays the individual participant data (very small dots) for each condition used to fit the model, overlaid with smoothed average curves. The fourth row shows the biases for each condition for the model fit (left) and the behavioral data (right). The behavioral data and color-coding for each range and condition are consistent with Figure 3 (red shades representing the egocentric and purple shades the allocentric condition). The resources are depicted in grey since they are utilized for both conditions. Within each panel, black horizontal lines indicate the respective stimulus headings, with a central black dot marking the midpoint of that range. Dashed grey vertical lines are used to highlight the three range centers at -35°, 0°, and 35°, and horizontal lines indicate the y = 0 axis. Blue curves within the prior distribution plots represent the expected shape based on the specific experimental stimulus range. The light grey background highlights the behavioral data.

Diving into the best fitted model, the reconstructed resources distributions showed a prominent peak at around 0° (straight-ahead) and this proved to be consistent across conditions and ranges by providing a better fit than allowing the resources to vary across the different conditions and ranges. For the egocentric condition, the derived prior distributions were unimodal and mimicked the physical distribution of presented headings, with the highest density of presented headings at around the center of the respective stimulus range (Figure 8). As expected by our rotation constraint, the peaks for the three ranges (left-centered, straight-ahead centered, and right-centered, respectively) were located at around: -35°, 0°, and 35°, respectively (Figure 8).

For the allocentric condition, there was a striking difference in the prior distribution, compared to the egocentric prior. While we also found a primary peak located at the same position as in the egocentric condition, its amplitude was significantly reduced. Furthermore, the allocentric prior featured smaller lateral peaks, resulting in a much more “flatter” prior distribution overall.

The common resources allocation and discrepancies in the priors are directly reflected in the modeled bias components. Even though the resources utilized by each condition are the same, the repulsion biases (driven by the resources) do not exhibit the exact same values due to sensory noise being fitted separately for each condition. However, as expected, the repulsion biases still remain very similar across conditions. We found clear differences in the attraction biases, particularly for the range centered at straight-ahead (Figure 8). Collectively, these modeling results indicate that the opposing heading biases observed in our experiments are not primarily due to changes in sensory sensitivity (resources allocation). Instead, they are mostly explained by a difference in the prior used to extract the heading percept in each task condition. This suggests that the “egocentric" vs. "allocentric" framing of the task fundamentally alters the internal

prediction the brain establishes to the incoming optic flow to eventually arrive at an estimate of the perceived heading direction.

Discussion

This study identifies the reference frame in which observers report their perceived heading as a central and previously overlooked determinant of biases in self-motion processing. With our behavioral experiment using a unique wide-field optic flow approach, we demonstrate that identical visual stimuli elicit centripetal biases when observers respond using an egocentric (self-centered) reference frame, but result in centrifugal biases when responses require an allocentric (world-centered) representation. Notably, these opposing effects were observed within the same exact participants.

Our findings provide an explanation for decades of conflicting reports in the literature on heading perception. Studies that required responses on a frontal-plane line (implicitly encouraging an egocentric representation) consistently reported centripetal errors. Conversely, experiments using circle-based response formats, which necessitate mapping the sensory input into an allocentric representation, reported centrifugal biases. Crucially, we show that these opposite biases persist even when the response range is held constant across conditions (ego- vs, allocentric), challenging the previous proposal that response-range alone accounts for the literature's contradictory findings[24].

Instead, our behavioral evidence suggests that the reference frame transformation is the primary driver of heading biases. Specifically, adopting an allocentric perspective requires a mental transformation of the retinal/egocentric optic flow pattern into a world-centered representation, and our results indicate that this transformation introduces the centrifugal biases observed in heading reports.

Our EEG results provide supporting neural evidence for this hypothesis. When participants prepared responses requiring an allocentric reference frame, we observed a robust increase in power at 7-16 Hz over parietal and posterior midline electrodes, compared to the egocentric condition. This frequency range overlaps with the theta-alpha band often associated with retrosplenial, parahippocampal, and hippocampal network engagement during navigation, involving spatial transformations and viewpoint changes[26,38–42]. This increase in the theta-alpha

power during the allocentric compared to the egocentric cue period, occurring in the absence of any visual stimulus changes, suggests that participants were actively performing a reference frame transformation in anticipation of the probe, triggered by the response cue. Together, the convergent behavioral and neural results strongly support the idea that the reference frame transformation itself, and not the extent of the response range, induces an opposite bias.

Our computational modeling shows that the divergence between egocentric and allocentric reports is largely explained by the difference in the prior distribution used for each condition. For the egocentric estimates, participants appear to learn the experimental stimulus distribution and rely heavily on this unimodal prior for their reports. In contrast, the allocentric condition is characterized by a "flatter" reconstructed prior. This indicates that for the “bird’s-eye view” judgements, participants do not rely solely on the experimental stimulus range, but instead assume the stimuli are more evenly distributed around the arc of possible responses. This could mean that they integrate the prior of the experimental stimulus with a long-term “natural-world” prior, where possible navigation directions are more broadly distributed across the full spectrum of forward directions.

The reduction in the difference between egocentric and allocentric biases in Experiment 1B likely reflects two additional factors: the closer proximity between the stimulus and the response range boundaries, and the asymmetric prior expectations introduced by the left- or right-shifted heading distributions. By shifting the prior to the center of the lateralized stimulus ranges, our model generated attraction biases that are more similar across conditions than those found in the straight-ahead centered range (Figure 8). These influences highlight that while reference frame transformations play a dominant role, heading biases can still be modulated by contextual factors such as range adaptation, or boundary effects. Importantly, however, these factors cannot account for the reversal of bias we reliably observed across reference frames when considering the straight-ahead centered stimulus range.

Regarding the underlying neural mechanisms of these biases, our model’s resources distribution (square root of the Fisher information) shows a clear peak at approximately 0°. This indicates better discriminability for headings close to straight-ahead as compared to lateral headings, consistent with the population Fisher information reported for areas MST[36] and VIP[16,37], as well as previous behavioral heading discrimination studies[23,43] and is in line with the statistical distribution of headings observed in natural (or virtual) environments[44,45]. While we might expect an additional resources peak at ±180° based on neural data from MST[36], our stimulus headings

were only up to ±90° for the lateralized ranges, which does not provide sufficient behavioral data to fully characterize these distributions beyond this range.

Together, our findings advance our understanding of heading perception: biases depend critically on the coordinate system in which an observer expresses their judgment. This finding has implications beyond self-motion perception. Many perceptual and cognitive tasks, from mental rotation to scene recognition and navigation, require reference frame transformations. While previous studies have investigated how this affects performance error[46–48], they have not, to our knowledge, compared centrifugal/centripetal biases with reference frames transformations. Our results also underscore the importance of describing and accounting for response formats in detail when comparing perceptual performance, particularly in studies involving spatial or navigational judgments.

Future work should investigate the neural mechanisms underlying these reference frame transformations in greater detail. Based on our modeling results, we hypothesize that the population Fisher information remains relatively stable to the Fisher information used for egocentric percepts, but the experimental prior is either de-weighted or combined with a long-term prior during the egocentric-to-allocentric transformation, for the centrifugal biases observed in the allocentric condition to arise. Testing this hypothesis will require neural recordings across the areas involved in the ego- to allocentric reference frame transformations, like the parietal and retrosplenial cortices, and (para-)hippocampal areas[26–28]. Additionally, exploring how these processes unfold in naturalistic virtual environments, where participants physically move and reorient, may reveal how reference frame transformations interact with other sensory signals, e.g. vestibular and proprioceptive.

Methods

Experiment 1A (Behavioral)

Participants

Forty participants (23 female, aged between 18 and 29, mean 20.15 years), who were naïve concerning the goal of the experiment and with no known neurological disorders were recruited from the Kinesiology Undergraduate Research Experience (KURE) at York University, Toronto, and were given course credit for participating in the study. All had normal or corrected-to-normal vision (with contact lenses, since we asked them not to wear glasses with visible frames which could have served as landmarks in their field of view). Data from three of them were excluded from further analysis, because participants failed to perform the task as intended. Prior to the experiment they provided written informed consent. Our study was in accordance with the Declaration of Helsinki and was approved by the Office of Research Ethics at York University.

Setup

Participants sat in a darkened room, centered in front of the Christie® Edgeless Graphics Geometry (EGG) visualization system, a large-field, curved screen with a field of view (FOV) of ±112° horizontally, and +89° and −83° vertically (see Figure 1 in McManus et al.[49] for a schematic). The screen had an 18-megapixel resolution, with an optical resolution of 6 arcmin/(Optical Line Pair). The EGG is also equipped with the Christie Twist™ attachment that improves the visual output from multiple projectors by adjusting warping and performing edge-blending. The distance between the participants and the screen was approximately 107cm and they viewed the stimulus binocularly.

Stimulus and task

The stimulus consisted of a plane of random dots shown in black over a light gray background (as in Figure 1) showing one of 9 possible headings: 0º, ±10º, ±20º, ±35º, ±55º for 600ms. Negative values indicate headings towards the left of the display center and vice versa. After the self-motion stimulus, one out of three possible reporting options appeared on the screen: egocentric, allocentric arc or allocentric circle. Participants were instructed to indicate the direction of their perceived heading from their point of view on a horizontal line (egocentric condition) or indicate the angle corresponding to their perceived heading seen from above (‘birds-eye-view’, both allocentric conditions). The difference between the two allocentric conditions resulted from

the available response range. In the allocentric circle condition, the response range was maximum, i.e. ±180° with respect to straight-ahead (corresponding to 0°). In the allocentric arc condition, the response range was identical to the response range in the egocentric condition, i.e. ±110°.

During the presentation of the self-motion stimulus, a fixation dot was shown in red, 2 meters away from the participant, with a radius of 3 cm, corresponding to 0.86 degrees, straight ahead of them at eye level. The plane of random dots was shown as being 2.5 m below the fixation dot in polar coordinates as follows: 5000 dots were distributed radially in a gaussian distribution (μ=100m from the observer, σ=45m) and angularly in a uniform distribution between -110º and 110º. (This generated a random distribution that had similar density in whichever direction the participants moved.) At any point participants could only see up to 60m ahead of them and they virtually moved 30m in one of the possible headings for each self-motion stimulus. Each black dot had a radius of 10 cm corresponding to approximately 0.1 degrees when being 60m away, up to 5 degrees when closest to the observer.

Each participant completed two experimental sets. In the first set, after the self-motion stimulus, participants were only presented with either the egocentric condition or the allocentric circle condition. In the second set, participants were presented with the three conditions, i.e. the previous two and the allocentric arc condition. In each of the sets the experiment consisted of 8 blocks per condition (only one of the conditions in an individual block) with 9 trials per block (one for each heading). Set 1 consisted of 16 blocks with a total of 144 trials, and Set 2 of 24 blocks with a total of 216 trials. The order of blocks for each participant was randomized.

The stimulus was programmed and displayed with Vizard 7 (version 7.2-dev2) using Python (version 3.8.0).

Data Analysis

Behavioral responses from N = 37 participants were analyzed. For each participant, condition, and self-motion direction, response bias was computed as: *Bias = reported self-motion direction – presented self-motion direction*. A positive bias indicated that the participant reported their perceived heading being towards the right of the real heading, while a negative bias corresponded to the participant reporting their perceived heading being towards the left of the presented

heading. A bias of 0° would indicate veridical performance. The bias was computed separately for Sets 1 and 2.

To test whether biases differed between experimental sets, paired two-tailed Wilcoxon signed-rank tests (*signrank*) were applied at each stimulus heading and for each condition, comparing bias means and standard deviations (SDs). A Bonferroni correction was applied across the nine stimulus headings.

To determine whether participants' biases were significantly different from 0, separate tests were performed for Sets 1 and 2. For each condition and self-motion direction, a two-tailed Wilcoxon signed-rank test compared the participant-level bias distribution against zero. Bonferroni correction was applied across stimulus headings.

Lastly, we compared the mean bias between the egocentric and allocentric conditions. Data from Set 1 and Set 2 were averaged and a paired two-tailed Wilcoxon signed-rank test was applied at each stimulus heading. The same procedure was applied to statistically test standard deviations (SDs) of the participants' responses, and Bonferroni correction was applied for means and SDs across stimulus headings.

Experiment 1B (Behavioral)

Participants

For a second version of the experiment with stimulus ranges not centered on straight-ahead but shifted to the left or to the right, twenty naïve participants (10 for each version: 6 female, all participants aged between 18 and 26, mean 19.8 years for the left-centered version and 7 female, all participants aged between 18 and 22. mean 19.5 years for the right-centered version) with no known neurological disorders were recruited from the Kinesiology Undergraduate Research Experience (KURE) at York University and were given course credit for participating in the study. All had normal or corrected-to-normal vision (with contact lenses). Data from one of them was excluded from further analysis, because the participant failed to perform the task as intended. Prior to the experiment all participants provided written informed consent. Like for Experiment 1A, our study was in accordance with the Declaration of Helsinki and was approved by the Office of Research Ethics at York University.

Setup, stimulus and task

The setup, the stimuli and the behavioral conditions were identical to experiment 1A. The only difference being that heading ranges were rotated by 35° to either the left (for the left-centered version) or the right (for the right-centered version) of the participant. This shifted the heading range to -90° to 20° and -20° to 90°, respectively. Each participant was presented with only one of those two ranges, either the left-centered or the right-centered, but not both. The fixation dot remained at the center of the screen at 0° for all experiments.

The task for the participants was the same as in experiment 1A, but participants were presented with only the egocentric condition or the allocentric arc (no allocentric circle). The experiment consisted of 2 sets and each of the sets consisted of 8 blocks per condition. There were 9 trials of the respective condition in each block. This gives a total of 9×8×2 = 144 trials per condition, for a grand total of 288 trials per participant.

Like before, the stimulus was programmed and displayed with Vizard 7 (v7.2-dev2) using Python (v3.8.0). The statistical analysis of the data was identical to experiment 1A.

Experiment 2 (EEG)

Participants

Twenty-one naïve participants (9 female, aged between 19 and 31, mean 22.47 years) with no known neurological disorders and normal or corrected-to-normal vision participated in our experiment and were compensated with 10 € per hour. Prior to the experiment they provided written informed consent. Our study was in accordance with the Declaration of Helsinki and was approved by the local Ethics Committee (Psychology Department, Marburg University).

Setup

Participants sat in a darkened and sound attenuated room. The stimuli were presented on a 24-inch computer monitor (VPixx Technologies Inc., Saint-Bruno, QC, Canada) 68 cm in front of them

at eye level. The participants' heads were stabilized by a chin rest. The display was 44° wide and 24.8° high and was set to a resolution of 1920 × 1080 pixels at a refresh rate of 120 Hz. Eye movements were recorded using an EyeLink 1000 system (SR Research, ON, Canada).

Electrophysiological recordings

We performed continuous electroencephalographic recordings (EEG) throughout the experiment using an actiCHamp module (Brain Products GmbH) and the software BrainVision PyCorder (Brain Vision LLC). We used 64 active Ag/AgCl electrodes according to the extended international 10–20 system on the participants' heads. Typically, the impedances of all electrodes were kept below 5 kΩ during the whole experiment. Electrode Cz was used as the reference electrode. The continuously recorded EEG signals were digitized at a sampling rate of 1000 Hz.

Stimulus and task

Participants performed a heading discrimination task in which a visually simulated self-motion direction was compared with a subsequently presented static direction. Each trial consisted of four sequential phases: self-motion stimulus, cue, probe, and feedback (Figure 4).

The self-motion stimuli comprised a ground plane of white random dots on a black background, simulating forward self-motion with a pseudo randomly selected heading direction between −15° and +15° in 1° increments. Stimulus duration varied randomly between 500 and 700 ms. Participants maintained fixation on a central red dot (0.3° diameter) throughout stimulus presentation.

Following a given self-motion stimulus, a cue was presented for 2200–2800 ms to indicate the reference frame for the upcoming discrimination. The cue was a blue square for the egocentric condition and a magenta circle in the allocentric condition. This cue period was used for EEG analyses.

The probe stimulus represented a directional offset relative to the previously presented heading (self-motion heading plus offset; redrawn if outside screen limits). In the egocentric condition, the probe was displayed as a vertical bar on a horizontal line; in the allocentric condition, it was displayed as a bar on a circular outline (Figure 4). In the allocentric display, a boldened arc

indicated the portion of the circle corresponding to the screen width (in the egocentric condition) transformed into allocentric coordinates. Across trials, probe offsets were randomly chosen from these values: 0°, ±5°, ±10°, or ±20°.

Participants indicated whether the probe was to the left or right of the self-motion heading via key press (left or right arrow keys, respectively), responding as quickly as possible. Probe duration was individually adjusted to allow in-time-responses on approximately 80% of the trials, maintaining task difficulty across participants. Feedback was provided at the end of each trial and was randomized for zero-offset trials.

Each participant completed two sessions of 200 trials each (100 egocentric, 100 allocentric), yielding 400 trials in total. Stimuli were generated and presented using MATLAB R2012a (MathWorks) and the psychophysics toolbox[50–52].

Behavioral performance

The proportion of correct/incorrect and timed-out responses across participants were tested for statistical difference using a Wilcoxon signed rank test. For all analyses, a value of $p \leq 0.05$ was used to determine statistical significance.

EEG preprocessing

Analysis of EEG data was performed offline using own scripts and the Fieldtrip toolbox[53] in MATLAB (MathWorks). The data was bandpass filtered between 2 and 100 Hz with addition of a notch filter at 50 Hz. Noisy electrodes were manually detected and excluded from the independent component analysis (ICA). ICA was performed immediately after, and eye-movement and other artifactual components were manually detected and respective trials removed from further data analysis. Noisy electrodes were interpolated after the artifacts were removed. The data was re-referenced to the average of all electrodes and epoched from -2000 ms before cue onset to 3000ms after cue onset with a baseline of -100 ms to 0 ms, right before cue onset. Individual noisy trials were manually rejected.

Time-frequency analysis

Time-frequency representations were computed based on complex Morlet wavelets using the function *ft_freqanalysis* from the Fieldtrip toolbox[53] in MATLAB. Frequencies of interest were defined from 1 to 30 Hz in increments of 0.5 Hz, and the time was sampled from -2 to +3 seconds around cue onset sampled at 50ms intervals. (ft_freqanalysis parameters: foi = 1:0.5:30, toi = -2:0.05:3. method = 'wavelet', pad = 'nextpow2', t_ftimwin = 3 /foi, tapsmofrq = foi*0.2, output = 'pow', keeptrials = 'yes')

Baseline correction was applied on a trial-by-trial basis in MATLAB using a custom code based on Ciuparu and Mureşan, 2016[54], first calculating the logarithm (base 10) of the power for each frequency and then z-scored using the average and standard deviation of a baseline segment from -500 to -100 ms before cue onset, calculated considering all trials from both conditions.

The time-frequency data was then averaged for each subject and condition.

Statistical analysis

For the statistical comparison between egocentric and allocentric conditions, we used FieldTrip's nonparametric cluster-based permutation framework[55]. Neighboring electrodes were defined using a distance-based spatial neighborhood structure, using the standard 64-channel actiCAP layout.

Cluster-based statistics were then computed including all EEG channels over a window of -500 to 2000 ms around cue onset, across all frequencies from 1 to 30 Hz. We performed a pairwise comparison between both conditions using a Monte-Carlo permutation method with a dependent-samples *t*-statistic. (Nperms = 5000, initial threshold of α=0.02 to consider a sample part of a cluster, minimum of 2 adjacent channels, clusterstatistic = "maxsum", two-tail correction = "prob" which multiplies the uncorrected probability by two before setting a threshold of α=0.05).

Modeling methods

We implemented a computational model based on the unifying theory of perceptual biases proposed by Hahn & Wei[35]. The model assumes that perception, in this case heading perception,

is governed by the interaction between a prior distribution of a stimulus θ, $p(\theta)$, and a sensory likelihood function, $p(m|\theta)$, where m represents the internal sensory representation of θ.

Following the efficient coding theory, the mapping between the physical stimulus space and the internal representation of the stimulus space, $F(\theta)$ can be non-linear, with, for example, small changes in headings close to straight-ahead, corresponding to large changes in the sensory representation. From this mapping, we can derive the distribution of "resources" allocated to different portions of the domain of θ (physical/stimulus domain), corresponding to the square root of the Fisher information. This distribution determines the local precision of the sensory measurements across the stimulus space; high resources density indicates high sensitivity (low discrimination thresholds), while low density indicates low sensitivity (high thresholds). Physiologically, the population Fisher information (and therefore the square of the resources) can be thought of as the derivative of tuning curves within neuronal populations responsive to visual self-motion stimuli[16,36,37].

In [35], Hahn & Wei demonstrate that the non-uniform resources allocation is the direct cause of repulsive biases that "push" the decoded estimates away from the areas of high resources density; by making the likelihood function become asymmetric (the effect of asymmetric likelihood functions has also previously been described in [56]). The total bias is then a combination of an attractive bias towards the peak of the prior (as in classical Bayesian inference models) and a repulsive bias away from the peak of the resources distribution (away from the peak of population Fisher information). The relative contribution of these biases towards the total bias is determined by the exponent of the loss function used to decode the percept. The goal of our model was to reconstruct the specific prior and resources distributions required to generate the observed behavioral biases used as input.

For the implementation, we fitted the egocentric and allocentric arc conditions for Experiments 1A and 1B. For both conditions, the stimulus and sensory spaces were discretized into a circular grid of 180 points to facilitate numerical integration. For encoding, the transfer function $F(\theta)$ was computed as the cumulative sum of the resources allocation, mapping the stimulus space into the sensory space. For decoding, we utilized a custom cosine estimator as described in [35], as it proved to converge better for our (angular) data. Therefore, the loss function was defined as: $\ell(\hat{\theta}, \theta) = (1 - cos(\hat{\theta} - \theta))^{p/2}$, where $\hat{\theta}$ is the perceptual estimate and θ is the heading stimulus. To account for the boundaries of the response range, the prior was truncated at ±110° and forced to be zero for all greater eccentricities. The final response distribution incorporated motor variance

and a “guessing rate” modeled via a mixture logit transform, to account for uniform response lapses.

The parameters were optimized using Gradient Descend (GD) by minimizing the negative log-likelihood (NLL) of the observed human responses. To prevent overfitting and ensure biological plausibility, we applied a regularization term based on the squared differences between adjacent points in the resources and prior distributions. 90% of the trials were used for model fitting and the remaining 10% for estimating held-out NLL.

We compared several model configurations to identify the one that best captured the observed bias differences while maintaining biological plausibility. Specifically, we tested the following four constraints:

a) Resources invariance across ranges: The resources distribution was constrained to remain constant across all three stimulus ranges within a given condition.

b) Resources invariance across conditions: The resources distribution was constrained to be identical for both the egocentric and allocentric conditions.

c) Prior invariance across ranges (rotated): The prior distribution was constrained to remain constant across the three stimulus ranges but was rotated by ±35° to align with the experimental shift in stimulus presentation.

d) Prior invariance across conditions: The prior distribution was constrained to be identical for both the egocentric and allocentric conditions.

By systematically testing these constraints, we were able to determine the degree to which the observed biases were driven by stable resources allocation versus stimulus- or condition-dependent changes in prior expectations. Model selection for constraints and loss function exponent was based on the comparison of the NLL on held-out data.

Data Availability

The datasets and analysis codes generated for both experiments during the current study are available in the following repository: https://tam-datahub.online.uni-marburg.de/handle/tam/56.

The code for the computational model can be found in the following repository: https://github.com/RenateRB/headingbiases/.

.

References

1. Warren, W. H. Optic Flow. in *The Senses: A Comprehensive Reference* 219–230 (Elsevier, 2008). doi:10.1016/B978-012370880-9.00311-X.
2. Gibson, J. J. *The Perception of the Visual World. The perception of the visual world.* (Houghton Mifflin, Oxford, England, 1950).
3. Warren, W. H. & Hannon, D. J. Direction of self-motion is perceived from optical flow. *Nature* **336**, 162–163 (1988).
4. Lappe, M., Bremmer, F. & Van Den Berg, A. V. Perception of self-motion from visual flow. *Trends Cogn. Sci.* **3**, 329–336 (1999).
5. Campbell, M. G. *et al.* Principles governing the integration of landmark and self-motion cues in entorhinal cortical codes for navigation. *Nat. Neurosci.* **21**, 1096–1106 (2018).
6. Prokop, T., Schubert, M. & Berger, W. Visual influence on human locomotion: Modulation to changes in optic flow. *Exp. Brain Res.* **114**, 63–70 (1997).
7. Frenz, H., Bremmer, F. & Lappe, M. Discrimination of travel distances from 'situated' optic flow. *Vision Res.* **43**, 2173–2183 (2003).
8. Bremmer, F. & Lappe, M. The use of optical velocities for distance discrimination and reproduction during visually simulated self motion. *Exp. Brain Res.* **127**, 33–42 (1999).
9. Churan, J., Paul, J., Klingenhoefer, S. & Bremmer, F. Integration of visual and tactile information in reproduction of traveled distance. *Journal of Neurophisiology* **118**, 1650–1663 (2017).
10. Von Hopffgarten, A. & Bremmer, F. Self-motion reproduction can be affected by associated auditory cues. *Seeing Perceiving* **24**, 203–222 (2011).
11. Mao, D. & Gu, Y. Multisensory coding of self-motion and its contribution to navigation. *Nat. Rev. Neurosci.* **26**, 715–732 (2025).
12. Royden, C. S., Banks, M. S. & Crowell, J. A. The perception of heading during eye movements. *Nature* 583–585 (1992) doi:10.1038/360583a0.
13. Sun, Q., Yan, R., Wang, J. & Li, X. Heading perception from optic flow is affected by heading distribution. *IPerception* **13**, (2022).
14. Sun, Q., Zhang, H., Alais, D. & Li, L. Serial dependence and center bias in heading perception from optic flow. *J. Vis.* **20**, 1–15 (2020).
15. Xu, L. H., Sun, Q., Zhang, B. & Li, X. Attractive serial dependence in heading perception from optic flow occurs at the perceptual and postperceptual stages. *J. Vis.* **22**, 1–25 (2022).
16. Bremmer, F., Churan, J. & Lappe, M. Heading representations in primates are compressed by saccades. *Nat. Commun.* **8**, 920 (2017).
17. Rosenblum, L., Kreß, A., Schwenk, J. C. B. & Bremmer, F. Visuo-tactile heading perception. *J. Neurophysiol.* **128**, 1355–1364 (2022).
18. Rosenblum, L., Grewe, E., Churan, J. & Bremmer, F. Influence of Tactile Flow on Visual Heading Perception. *Multisens. Res.* **35**, 291–308 (2022).
19. D'Avossa, G. & Kersten, D. Evidence in Human Subjects for Independent Coding of Azimuth and Elevation for Direction of Heading from Optic Flow. *Vision Res.* **36**, 2915–2924 (1996).

20. Xing, X. & Saunders, J. Center bias in perceived heading from optic flow. *J. Vis.* **16**, 884 (2016).
21. Crane, B. T. Coordinates of human visual and inertial heading perception. *PLoS One* **10**, 1–14 (2015).
22. Crane, B. T. Direction Specific Biases in Human Visual and Vestibular Heading Perception. *PLoS One* **7**, 1–15 (2012).
23. Cuturi, L. F. & MacNeilage, P. R. Systematic Biases in Human Heading Estimation. *PLoS One* **8**, e56862 (2013).
24. Sun, Q., Xu, L.-H. & Stocker, A. A. A linear perception-action mapping accounts for response range-dependent biases in heading estimation from optic flow. *PLoS Comput. Biol.* **21**, e1013147 (2025).
25. Reisenegger, R., Bansal, A., Harris, L. R. & Bremmer, F. Conflicting heading biases explained by different reference frames. *J. Vis.* **25**, 2595 (2025).
26. Alexander, A. S., Robinson, J. C., Stern, C. E. & Hasselmo, M. E. Gated transformations from egocentric to allocentric reference frames involving retrosplenial cortex, entorhinal cortex, and hippocampus. *Hippocampus* **33**, 465–487 (2023).
27. Bicanski, A. & Burgess, N. A neural-level model of spatial memory and imagery. *Elife* https://doi.org/10.7554/eLife.33752.001 (2018) doi:10.7554/eLife.33752.001.
28. Byrne, P., Becker, S. & Burgess, N. Remembering the past and imagining the future: A neural model of spatial memory and imagery. *Psychol. Rev.* **114**, 340–375 (2007).
29. Rolls, E. T. Neurons including hippocampal spatial view cells, and navigation in primates including humans. *Hippocampus* **31**, 593–611 (2021).
30. Rolls, E. T. Spatial coordinate transforms linking the allocentric hippocampal and egocentric parietal primate brain systems for memory, action in space, and navigation. *Hippocampus* **30**, 332–353 (2020).
31. Clark, B. J. *et al.* The Retrosplenial-Parietal Network and Reference Frame Coordination for Spatial Navigation. *Behavioral Neuroscience* **132**, 416–429 (2019).
32. Vann, S. D., Aggleton, J. P. & Maguire, E. A. What does the retrosplenial cortex do? *Nat. Rev. Neurosci.* **10**, 792–802 (2009).
33. Alexander, A. S., Place, R., Starrett, M. J., Chrastil, E. R. & Nitz, D. A. Rethinking retrosplenial cortex: Perspectives and predictions. *Neuron* **111**, 150–175 (2023).
34. Alexander, A. S. & Nitz, D. A. Retrosplenial cortex maps the conjunction of internal and external spaces. *Nat. Neurosci.* **18**, 1143–1151 (2015).
35. Hahn, M. & Wei, X. X. A unifying theory explains seemingly contradictory biases in perceptual estimation. *Nat. Neurosci.* **27**, 793–804 (2024).
36. Gu, Y., Fetsch, C. R., Adeyemo, B., DeAngelis, G. C. & Angelaki, D. E. Decoding of MSTd population activity accounts for variations in the precision of heading perception. *Neuron* **66**, 596–609 (2010).
37. Chen, A., DeAngelis, G. C. & Angelaki, D. E. Representation of vestibular and visual cues to self-motion in ventral intraparietal cortex. *Journal of Neuroscience* **31**, 12036–12052 (2011).
38. Alexander, A. S., Rangel, L. M., Tingley, D. & Nitz, D. A. Neurophysiological signatures of temporal coordination between retrosplenial cortex and the hippocampal formation. *Behavioral Neuroscience* **132**, 453–468 (2018).

39. Hafting, T., Fyhn, M., Bonnevie, T., Moser, M. B. & Moser, E. I. Hippocampus-independent phase precession in entorhinal grid cells. *Nature* **453**, 1248–1252 (2008).
40. O'Keefe, J. & Recce, M. L. Phase relationship between hippocampal place units and the EEG theta rhythm. *Hippocampus* **3**, 317–330 (1993).
41. Goyal, A. *et al.* Functionally distinct high and low theta oscillations in the human hippocampus. *Nat. Commun.* **11**, 1–10 (2020).
42. Gramann, K. *et al.* Human Brain Dynamics Accompanying Use of Egocentric and Allocentric Reference Frames during Navigation. *J. Cogn. Neurosci.* **22**, 2836–2849 (2010).
43. Crowell, J. A. & Banks, M. S. Perceiving heading with different retinal regions and types of optic flow. *Percept. Psychophys.* **53**, 325–337 (1993).
44. Sinnott, C., Dang, T., Papachristos, C., Alexis, K. & MacNeilage, P. Statistical characterization of heading stimuli in natural environments using SLAM. *J. Vis.* **18**, 41 (2018).
45. Kreß, A., Lappe, M. & Bremmer, F. Comprehensive VR dataset for machine learning: Head- and eye-centred video and positional data. *Data in Brief* **57**, 111187 (2024).
46. Shelton, A. L. & McNamara, T. P. Systems of Spatial Reference in Human Memory. *Cogn. Psychol.* **43**, 274–310 (2001).
47. Wang, R. F. & Spelke, E. S. Human spatial representation: Insights from animals. *Trends in Cognitive Sciences* vol. 6 376–382 Preprint at https://doi.org/10.1016/S1364-6613(02)01961-7 (2002).
48. Burgess, N., Spiers, H. J. & Paleologou, E. Orientational manoeuvres in the dark: Dissociating allocentric and egocentric influences on spatial memory. *Cognition* **94**, 149–166 (2004).
49. McManus, M., D'Amour, S. & Harris, L. R. Using optic flow in the far peripheral field. *J. Vis.* **17**, 1–11 (2017).
50. Brainard, D. H. The Psychophysics Toolbox. *Spat. Vis.* **10**, 433–436 (1997).
51. Kleiner, M., Brainard, D. & Pelli, D. ECVP '07 Abstracts. *Perception* **36**, 1–235 (2007).
52. Pelli, D. G. The VideoToolbox software for visual psychophysics: transforming numbers into movies. *Spat. Vis.* **10**, 437–442 (1997).
53. Oostenveld, R., Fries, P., Maris, E. & Schoffelen, J.-M. FieldTrip: Open Source Software for Advanced Analysis of MEG, EEG, and Invasive Electrophysiological Data. *Comput. Intell. Neurosci.* **2011**, 1–9 (2011).
54. Ciuparu, A. & Mureşan, R. C. Sources of bias in single-trial normalization procedures. *European Journal of Neuroscience* **43**, 861–869 (2016).
55. Maris, E. & Oostenveld, R. Nonparametric statistical testing of EEG- and MEG-data. *J. Neurosci. Methods* **164**, 177–190 (2007).
56. Wei, X. X. & Stocker, A. A. A Bayesian observer model constrained by efficient coding can explain 'anti-Bayesian' percepts. *Nat. Neurosci.* **18**, 1509–1517 (2015).

Acknowledgements

This research was supported by the German Research Foundation (Deutsche Forschungsgemeinschaft, DFG: IRTG-1901 and CRC/TRR-135, project number 222641018; Excellence cluster The Adaptive Mind – TAM, project number 533717223), and the EU (PLACES). The EGG display was provided by the Canadian Foundation for Innovation.

LRH was supported by Discovery Grant RGPIN-2020-06093 from the Natural Sciences and Engineering Research Council of Canada. The Christie® Edgeless Graphics display was made possible by funding from the Canadian Foundation for Innovation (project #30859).

We thank Christopher Janas for conducting the EEG data collection.

Author contributions

R.R., L.R.H. and F.B. designed research; R.R. and A.B. performed the behavioral experiments; R.R. and M.H. performed the computational modeling; R.R. and N.S. analyzed EEG data; R.R., M.H., N.S., A.B., L.R.H. and F.B. interpreted results of experiments; R.R. prepared figures; R.R. and F.B. drafted manuscript; R.R., M.H., A.B., L.R.H. and F.B. edited and revised manuscript; L.R.H. and F.B. approved final version of manuscript.

Competing Interests

The authors declare no competing interests, financial or otherwise.

Tables

Heading stimulus (°)	Bias Mean Difference		Bias SD Difference	
	Mean ± SD (°)	*p*-values	Mean ± SD (°)	*p*-values
-55	-16.6 ± 17.0	**<0.0001**	2.5 ± 7.5	1
-35	-12.2 ± 12.9	**0.0001**	3.1 ± 5.5	**0.0103**
-20	-9.0 ± 8.0	**<0.0001**	3.1 ± 4.1	**0.0012**
-10	-5.9 ± 5.4	**<0.0001**	3.8 ± 4.3	**0.0001**
0	1.2 ± 1.8	**0.0027**	0.4 ± 2.1	1
10	7.6 ± 5.9	**<0.0001**	2.2 ± 3.5	**0.0010**
20	13.3 ± 7.6	**<0.0001**	3.0 ± 4.6	**0.0006**
35	15.9 ± 11.9	**<0.0001**	3.3 ± 4.9	**0.0006**
55	18.5 ± 16.2	**<0.0001**	2.0 ± 5.6	0.3684

Table 1. Ego- vs. allocentric circle bias (averaged across sets).

Comparison between egocentric and allocentric circle response biases, with responses averaged across Set 1 and Set 2. For each heading angle, the mean signed difference (mean ± standard deviation) is reported, together with the Bonferroni-corrected *p*-value from a Wilcoxon signed-rank test. Negative values indicate a more leftward bias of the allocentric condition compared to the egocentric one and positive values vice versa. The same analysis is reported for response variability (standard deviation). Each row represents a single heading angle. Significant Bonferroni-corrected *p*-values ($p < 0.05$) are shown in bold. (*p*-values also shown in Figure 2 as black asterisks)

Head. stim. (°)	Set 1				Set 2					
	Egocentric		Allocentric Circle		Egocentric		Allocentric Circle		Allocentric Arc	
	Mean ± SD (°)	*p*-values	Mean ± SD (°)	*p*-values	Mean ± SD (°)	*p*-values	Mean ± SD (°)	*p*-values	Mean ± SD (°)	*p*-values
-55	16.5 ± 18.4	**0.0002**	1.5 ± 14.5	1	14.3 ± 17.0	**0.0005**	-3.9 ± 14.6	0.9731	-4.6 ± 14.8	0.8069
-35	7.5 ± 12.4	**0.0098**	-3.3 ± 9.7	0.4898	6.4 ± 11.5	**0.0401**	-7.2 ± 9.2	**0.0010**	-8.4 ± 10.7	**0.0009**
-20	1.6 ± 7.5	1	-6.6 ± 7.3	**0.0001**	0.3 ± 8.0	1	-9.4 ± 7.3	**<0.0001**	-8.6 ± 9.2	**0.0001**
-10	-0.7 ± 4.9	1	-6.4 ± 6.2	**<0.0001**	-2.7 ± 4.9	**0.0441**	-8.8 ± 6.2	**<0.0001**	-7.3 ± 6.7	**<0.0001**
0	-0.2 ± 2.2	1	1.2 ± 1.7	**0.0004**	-0.1 ± 1.3	1	0.9 ± 2.3	**0.0441**	1.0 ± 2.4	0.0871
10	0.4 ± 4.5	1	7.6 ± 6.0	**<0.0001**	1.8 ± 5.8	0.8069	9.9 ± 6.3	**<0.0001**	9.3 ± 6.3	**<0.0001**
20	-2.5 ± 7.8	0.5620	9.4 ± 7.6	**<0.0001**	-2.3 ± 7.0	0.7816	12.4 ± 8.9	**<0.0001**	11.6 ± 9.8	**<0.0001**
35	-7.7 ± 11.4	**0.0051**	6.7 ± 10.2	**0.0043**	-5.8 ± 11.8	**0.0484**	11.6 ± 11.1	**<0.0001**	12.0 ± 11.8	**<0.0001**
55	-15.7 ± 18.5	**0.0010**	2.0 ± 13.5	1	-12.3 ± 19.8	**0.0075**	6.9 ± 14.0	0.0531	7.0 ± 14.2	**0.0484**

Table 2. Comparison to zero bias.

One-sample Wilcoxon signed-rank tests assessing whether response biases significantly differ from zero for each heading angle. Analyses were performed separately for Set 1 and Set 2. For each heading, the table reports the mean bias (mean ± standard deviation) and the Bonferroni-corrected *p*-value. Each row corresponds to a single heading angle. Significant Bonferroni-corrected *p*-values ($p < 0.05$) are shown in bold. (*p*-values also shown in Figure 2 as colored asterisks)

Heading stimulus (°)	Bias mean		Bias SD	
	Mean ± SD (°)	*p*-values	Mean ± SD (°)	*p*-values
Leftward (n=9)				
-90	-10.9 ± 9.0	0.0703	-8.1 ± 14.8	0.3516
-70	-11.5 ± 8.3	**0.0352**	0.7 ± 5.0	1
-55	-8.1 ± 7.5	0.1758	4.3 ± 5.0	0.3516
-45	-5.2 ± 10.7	1	5.0 ± 4.0	0.0703
-35	-1.9 ± 8.5	1	1.2 ± 4.6	1
-25	-1.4 ± 7.7	1	1.7 ± 3.4	1
-15	-1.2 ± 4.9	1	0.3 ± 3.6	1
0	0.9 ± 1.9	1	0.6 ± 1.0	1
20	4.4 ± 7.2	1	-0.1 ± 4.5	1
Straight-ahead (n=37)				
-55	-18.8 ± 17.6	**<0.0001**	3.8 ± 9.4	0.2633
-35	-14.8 ± 13.6	**<0.0001**	2.8 ± 5.3	**0.0421**
-20	-9.0 ± 10.6	**0.0003**	2.7 ± 4.5	**0.0135**
-10	-4.7 ± 6.9	**0.0036**	3.0 ± 3.7	**0.0008**
0	1.1 ± 2.7	0.0609	1.8 ± 2.8	**0.0024**
10	7.5 ± 7.0	**<0.0001**	2.2 ± 4.4	0.0247
20	13.9 ± 9.4	**<0.0001**	3.0 ± 3.7	**0.0003**
35	17.8 ± 13.5	**<0.0001**	2.5 ± 5.7	0.2086
55	19.3 ± 17.7	**<0.0001**	1.5 ± 7.9	1
Rightward (n=10)				
-20	-7.6 ± 6.1	0.0527	1.4 ± 3.2	1
0	-0.2 ± 2.3	1	1.9 ± 1.7	**0.0176**
15	8.4 ± 5.1	**0.0176**	2.8 ± 5.7	1
25	10.4 ± 8.1	**0.0352**	1.4 ± 3.7	1
35	12.8 ± 11.7	0.0879	2.6 ± 2.4	0.0879
45	12.7 ± 11.9	0.0527	5.2 ± 6.3	0.0879
55	13.2 ± 12.8	**0.0352**	3.0 ± 6.4	1
70	14.7 ± 14.6	0.1230	1.4 ± 7.7	1
90	14.9 ± 14.1	0.0527	2.8 ± 9.4	1

Table 3. Egocentric vs allocentric arc bias.

Comparison between egocentric and allocentric response biases in the *leftward, rightward and straight-ahead* ranges, across stimulus heading angles. For each heading, the mean signed difference between egocentric and allocentric arc responses (mean ± standard deviation) is reported together with the Bonferroni-corrected *p*-value obtained from a Wilcoxon signed-rank test. Negative values indicate a more leftward bias of the allocentric condition compared to the

egocentric one and positive values vice versa. The same statistical comparison is provided for response variability (standard deviation). Rows correspond to individual heading angles. Significant Bonferroni-corrected *p*-values ($p < 0.05$) are shown in bold. (*p*-values for the differences of the mean also shown in Figure 3 as black asterisks).

Supplementary Material

Heading stimulus (°)	Egocentric				Allocentric Circle			
	Bias Mean Difference		Bias SD Difference		Bias Mean Difference		Bias SD Difference	
	Mean ± SD (°)	*p*-values	Mean ± SD (°)	*p*-values	Mean ± SD (°)	*p*-values	Mean ± SD (°)	*p*-values
-55	2.2 ± 10.1	1	0.0 ± 4.1	1	5.4 ± 13.2	0.178	-1.1 ± 10.4	1
-35	1.1 ± 7.6	1	0.9 ± 4.6	1	3.9 ± 10.4	0.193	0.1 ± 5.1	1
-20	1.3 ± 6.0	1	0.3 ± 3.6	1	2.7 ± 7.9	0.473	0.0 ± 6.2	1
-10	1.9 ± 4.1	0.095	0.2 ± 3.0	1	2.3 ± 6.1	1	0.3 ± 7.3	1
0	-0.2 ± 2.5	1	-0.2 ± 2.2	1	0.3 ± 2.4	1	-0.6 ± 3.3	0.973
10	-1.4 ± 5.3	1	0.2 ± 3.0	1	-2.2 ± 5.9	0.687	0.4 ± 4.7	1
20	-0.2 ± 4.2	1	0.5 ± 2.3	1	-2.9 ± 8.1	0.562	1.7 ± 8.7	1
35	-1.9 ± 8.4	1	0.1 ± 3.3	1	-5.9 ± 11.3	0.158	-1.1 ± 7.2	1
55	-3.5 ± 10.3	0.833	-1.5 ± 6.8	1	-4.9 ± 13.3	0.342	-1.4 ± 9.0	1

Supplementary Table 1. Comparison between experimental sets (Set 1 vs Set 2).

Comparison of response biases between Set 1 and Set 2 of the experiment for each heading angle and condition. The mean signed difference between Set 1 and Set 2 responses (mean ± standard deviation) is reported, along with the Bonferroni-corrected *p*-values from a Wilcoxon signed-rank test. An analogous analysis is provided for the standard deviation of responses. Rows correspond to individual heading angles.